

FaceScape: a Large-scale High Quality 3D Face Dataset and Detailed Riggable 3D Face Prediction

Haotian Yang^{*1} Hao Zhu^{*1,2,5} Yanru Wang¹ Mingkai Huang¹

Qiu Shen¹ Ruigang Yang^{2,3,4,5} Xun Cao¹

¹Nanjing University ²Baidu Research ³University of Kentucky ⁴Inceptio Inc.

⁵National Engineering Laboratory for Deep Learning Technology and Applications, China

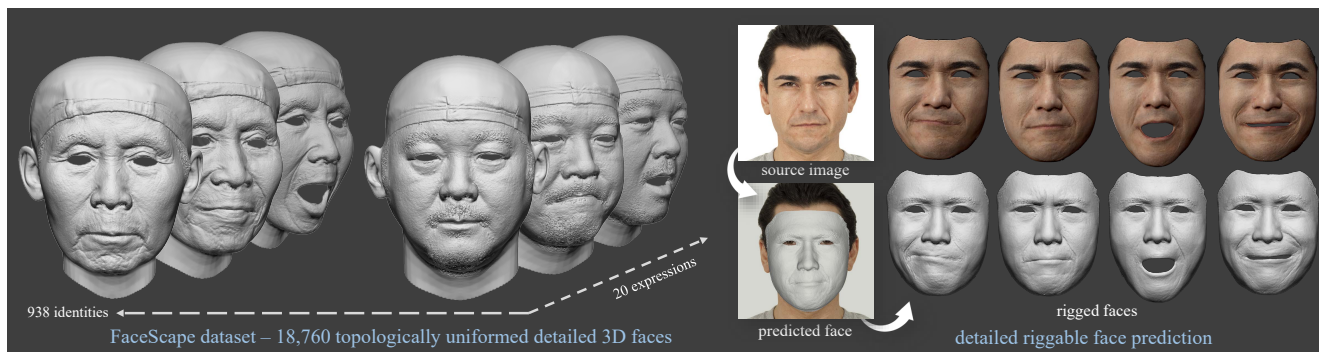


Figure 1: We present FaceScape, a large-scale detailed 3D face dataset consisting of 18,760 textured 3D face models with pore-level geometry. By learning dynamic details from FaceScape, we present a novel algorithm to predict from a single image a detailed **riggable** 3D face model that can generate various expressions with high geometric details.

Abstract

In this paper, we present a large-scale detailed 3D face dataset, FaceScape, and propose a novel algorithm that is able to predict elaborate riggable 3D face models from a single image input. FaceScape dataset provides 18,760 textured 3D faces, captured from 938 subjects and each with 20 specific expressions. The 3D models contain the pore-level facial geometry that is also processed to be topologically uniformed. These fine 3D facial models can be represented as a 3D morphable model for rough shapes and displacement maps for detailed geometry. Taking advantage of the large-scale and high-accuracy dataset, a novel algorithm is further proposed to learn the expression-specific dynamic details using a deep neural network. The learned relationship serves as the foundation of our 3D face prediction system from a single image input. Different than the previous methods, our predicted 3D models are riggable with highly detailed geometry under different expressions. The unprecedented dataset and code will be released to public for research purpose[†].

* These authors contributed equally to this work.

† <https://github.com/zhuhao-nju/facescape.git>

1. Introduction

Parsing and recovering 3D face models from images have been a hot research topic in both computer vision and computer graphics due to its many applications. As learning based methods have become the mainstream in face tracking, recognition, reconstruction and synthesis, 3D face datasets becomes increasingly important. While there are numerous 2D face datasets, the few 3D datasets lack in 3D details and scale. As such, learning-based methods that rely on the 3D information suffer.

Existing 3D face datasets capture the face geometry using sparse camera array[8, 19, 35] or active depth sensor such as Kinect[12] and coded light[34]. These setups limit the quality of the recovered faces. We captured the 3D face model using a dense 68-camera array under controlled illumination, which recovers the 3D face model with wrinkle and pore level detailed shapes, as shown in Figure 1. In addition to shape quality, our dataset provides considerable amount of scans for study. We invited 938 people between the ages of 16 and 70 as subjects, and each subject is guided to perform 20 specified expressions, generating 18,760 high quality 3D face models. The corresponding color images and subjects' basic information (such as age and gender)

are also recorded.

Based on the high fidelity raw data, we build a powerful parametric model to represent the detailed face shape. All the raw scans are firstly transformed to a topologically uniformed base model representing the rough shape and a displacement map representing detailed shape. The transformed models are further used to build bilinear models in identity and expression dimension. Experiments show that our generated bilinear model exceeds previous methods in representative ability.

Using FaceScape dataset, we study how to predict a detailed riggable face model from a single image. Prior methods are able to estimate rough blendshapes where no wrinkle and subtle features are recovered. The main problem is how to predict the variation of small-scale geometry caused by expression changing, such as wrinkles. We propose the dynamic details which can be predicted from a single image by training a deep neural network on FaceScape dataset. Cooperated with bilinear model fitting method, a full system to predict detailed riggable model is presented. Our system consists of three stages: base model fitting, displacement map prediction and dynamic details synthesis. As shown in Figure 1, our method predicts detailed 3D face model which contains subtle geometry, and achieves high accuracy due to the powerful bilinear model generated from FaceScape dataset. The predicted model can be rigged to various expressions with plausible detailed geometry.

Our contributions are summarized as following:

- We present a large-scale 3D face dataset, FaceScape, consisting of 18,760 extremely detailed 3D face models. All the models are processed to topologically uniformed base models for rough shape and displacement maps for detailed shape. The data are released free for non-commercial research.
- We model the variation of detailed geometry acrossing expressions as dynamic details, and propose to learn the dynamic detail from FaceScape using a deep neural network.
- A full pipeline is presented to predict detailed riggable face model from a single image. Our result model can be rigged to various expressions with plausible geometric details.

2. Related Work

3D Face Dataset. 3D face datasets are of great value in face-related research areas. Existing 3D face datasets could be categorized according to the acquisition of 3D face model. Model fitting datasets[34, 63, 24, 5, 7] fit the 3D morphable model to the collected images, which makes it convenient to build a large-scale dataset on the base of wild faces. The major problem of the fitted 3D model is

the uncertainty of accuracy and the lack of detailed shape. To obtain the accurate 3D face shape, a number of works reconstructed the 3D face using active method including depth sensor or scanner[56, 55, 3, 40, 39, 12, 17], while the other works built sparse multi-view camera system[57, 18]. Traditional depth sensors and 3D scanners suffer from the limited spatial resolution, so they can't recover detailed facial geometry. The sparse multi-view camera system suffers from the unstable and inaccurate reconstruction[41, 59, 58]. The drawbacks of these methods limit the quality of 3D face model in previous datasets. Different from the datasets above, FaceScape obtained the 3D face model from a dense multi-view system with 68 DSLR cameras, which provides extremely high quality face models. The parameters measuring 3D model quality are listed in Table 1. Our dataset outperforms previous works on both model quality and data amount. Note that Table 1 doesn't list the datasets which provide only parametric model but no source 3D models[8, 6, 34, 31].

3D Morphable Model. 3DMM is a statistical model which transforms the shape and texture of the faces into a vector space representation[4]. As 3DMM inherently contains the explicit correspondences from model to model, it is widely used in model fitting, face synthesis, image manipulations, etc. The recent research on 3DMM can be generally divided into two directions. The first direction is to separate the parametric space to multiple dimensions like identity, expression and visemes, so that the model could be controlled by these attributes separately[52, 12, 30, 27]. The models in expression dimension could be further transformed to a set of blendshapes[28], which can be rigged to generate individual-specific animation. Another direction is to enhance the representation power of 3DMM by using deep neural network to present 3DMM bases [2, 45, 48, 50, 49, 16].

Single-view shape Prediction. Predicting 3D shape from a single image is a key problem to many applications like view synthesis[22, 60, 61] and stereoscopic video generation[13, 25]. The emergence of 3DMM has simplified the single-view reconstruction of face to a model fitting problem, which could be well solved by fitting facial landmarks and other features[38, 46] or regressing the parameter of 3DMM with a deep neural network[20, 63]. However, fitting 3DMM is difficult in recovering small details from the input image due to the limited representation power. To solve this problem, several recent works adopt the multi-layer refinement structures. Richardson *et al.* [37] and Sela *et al.* [42] both proposed to firstly predict a rough facial shape and render it to the depth map, then refine the depth map to enhance the details from the registered source image. Sengupta *et al.* [43] proposed to train the SfSNet on combination of labeled synthetic data and unlabeled in-the-wild data to estimate plausible detailed shape in un-

Table 1: Comparison of 3D Face Datasets

Dataset	Sub. Num	Exp. Num	Vert. Num	Image/Texture Resolution	Source
BU-3DFE[56]	100	25	10k-20k	1300 × 900 / -	structure light
BU-4DFE[55]	101	6(video)	10k-20k	1040 × 1329 / -	structure light
BJUT-3D[3]	500	1-3	≈200k	478 × 489 / -	laser scanner
Bosphorus[40]	105	35	≈35k	1600 × 1200 / -	structure light
FaceWarehouse[12]	150	20	≈11k	640 × 480 / -	kinect
4DFAB[17]	180	6(video)	≈100k	1200 × 1600 / -	kinect+cameras(7)
D3DFACS[18]	10	38AU(video)	≈30k	- / 1024 × 1280	multi-view system(6)
BP4D-Spontaneous[57]	41	27AU(video)	≈37k	1040 × 1392 / -	multi-view system(3)
FaceScape (Ours)	938	20	≈2m	4k-8k / 4096×4096	multi-view system(68)

constrained images. Tran *et al.* [47] proposed to predict a bump map to represent the wrinkle-level geometry base on a rough base model. Huynh *et al.* [26] utilized image-to-image network and super-resolution network to recover the mesoscopic facial geometry in the form of displacement map. Chen *et al.* [15] also tried to predict the displacement map with a conditional GAN based on the 3DMM model, which enables to recover detailed shape from an in-the-wild image.

Our work advances the state of the art in multiple aspects. In dataset, our FaceScape is by far the largest with the highest quality. A detailed quantitative comparison with previous datasets are made in Table 1. In 3D face prediction, previous works focus on enhancing the static detailed facial shape, while we study the problem of recovering an **animable** model from a single image. We demonstrate for the first time that a detailed and rigged 3D face model can be recovered from a single image. The rigged model exhibits expression-dependent geometric details such as wrinkles.

3. Dataset

3.1. 3D Face Capture

We use a multi-view 3D reconstruction system to capture the raw mesh model for the datasets. The multi-view system consists of 68 DSLR cameras, 30 of which capture 8K images focusing on front side, and the other cameras capture 4K level images for the side part. The camera shutters are synced to be triggered within 5ms. We spend six months to invite 938 people to be our capturing subjects. The subjects are between 16 and 70 years old, and are mostly from Asia. We follow FaceWarehouse[12] which asks each subject to perform 20 specific expressions including neutral expression for capturing. The total reconstructed number reach to roughly 18,760, which is the largest amount comparing to previous expression controlled 3D face datasets. The reconstructed model is triangle mesh with roughly 2 million vertices and 4 million triangle faces. The meta information for each subject is recorded, including age, gender, and job

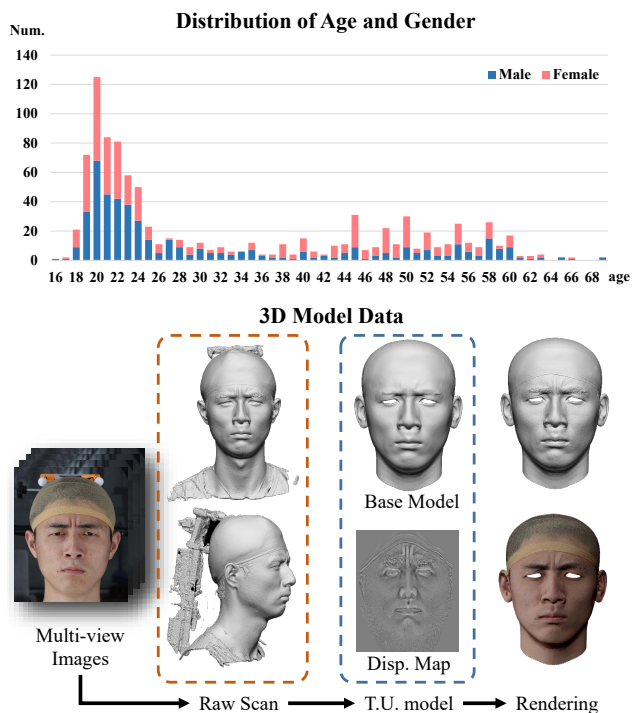


Figure 2: Description of FaceScape dataset. In the upper side we show the histogram of subjects’ age and gender. In the lower side we show the pipeline from the captured multi-view images to topologically uniformed models (T.U. models).

(by voluntary). We show the statistical information about the subjects in our dataset in Figure 2, and a comparison with prior 3D face datasets in Table 1.

3.2. Topologically Uniformed Model

We down-sample the raw recovered mesh into rough mesh with less triangle faces, namely base shape, and then build 3DMM for these simplified meshes. Firstly, we roughly register all the meshes to the template face model

by aligning 3D facial landmarks, then the NICP[1] is used to deform the templates to fit the scanned meshes. The deformed meshes can be used to represent the original scanned face with minor accuracy loss, and more importantly, all of the deformed models share the uniform topology. The detailed steps to register all the raw meshes are described in the supplementary material.

After obtaining the topology-uniformed base shape, we use displacement maps in UV space to represent middle and fine scale details that are not captured by the base model due to the small number of vertices and faces. We find the surface points of base mesh corresponding to the pixels in the displacement map, then inverse-project the points to the raw mesh along normal direction to find its corresponding points. The pixel values of the displacement map is set to the signed distance from the point on base mesh to its corresponding point.

We use base shapes to represent rough geometry and displacement maps to represent detailed geometry, which is a two-layer representation for our extremely detailed face shape. The new representation takes roughly 2% of the original mesh data size, while maintaining the mean absolute error to be less than 0.3mm.

3.3. Bilinear Model

Bilinear model is firstly proposed by Vlastic *et al.* [52], which is a special form of 3D morphable model to parameterize face models in both identity and expression dimensions. The bilinear model can be linked to a face-fitting algorithm to extract identity, and the fitted individual-specific model can be further transformed to riggable blendshapes. Here we describe how to generate bilinear model from our topologically uniformed models. Given 20 registered meshes in different expressions, we use the example based facial rigging algorithm[28] to generate 52 blendshapes based on FACS[21] for each person. Then we follow the previous methods[52, 12] to build the bilinear model from generated blendshapes in the space of $26317 \text{ vertices} \times 52 \text{ expressions} \times 938 \text{ identities}$. Specifically, we use Tucker decomposition to decompose the large rank-3 tensor to a small core tensor C_r and two low dimensional components for identity and expression. New face shape can be generated given the the identity parameter \mathbf{w}_{id} and expression parameter \mathbf{w}_{exp} as:

$$V = C_r \times \mathbf{w}_{exp} \times \mathbf{w}_{id} \quad (1)$$

where V is the vertex position of the generated mesh.

The superiority in quality and quantity of FaceScape makes the generated bilinear model own higher representation power. We evaluate the representation power of our model by fitting it to scanned 3D meshes not part of the training data. We compare our model to FaceWarehouse(FW)[12] and FLAME[30] by fitting them

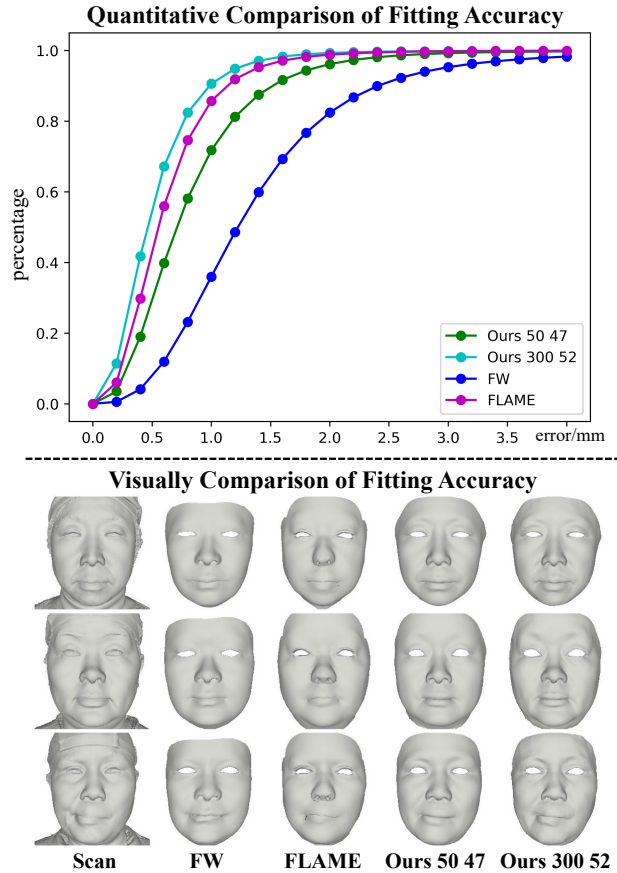


Figure 3: Comparison of Reconstruction Error for parametric model generated by FaceScape and previous datasets.

to our self-captured test set, which consists of 1000 high quality meshes from 50 subjects performing 20 different expressions each. FW has 50 identity parameters and 47 expression parameters, so we use the same number of parameters for fair comparison. To compare with FLAME which has 300 identity parameters and 100 expression parameters, we use 300 identity parameters and all 52 expression parameters. Figure 3 shows the cumulative reconstruction error. Our bilinear face model achieves much lower fitting error than FW using the same number of parameters and also outperform FLAME using even less expression parameters. The visually comparison in Figure 3 shows ours model could produce more mid-scale details than FW and FLAME, leading to more realistic fitting results.

4. Detailed Riggable Model Prediction

As reviewed in the related works in Section 2, existing methods have succeed in recovering extremely detailed 3D facial model from a single image. However, these recovered models are not riggable in expression space, since the recovered detail is static to the specific expression. Another

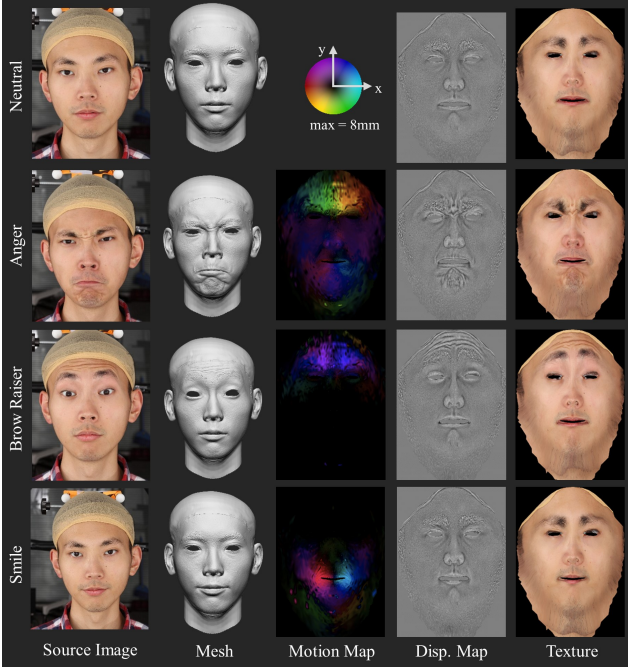


Figure 4: Riggable details can be decoupled as static details and dynamic details. The static details can be estimated from the facial textures, while the dynamic details are strongly related to the facial deforming map.

group of works try to fit a parametric model to the source image, which will obtain an expression-riggable model, but the recovered geometry stays in the rough stage.

The emerge of FaceScape dataset makes it possible to estimate detailed and riggable 3D face model from a single image, as we can learn the dynamic details from the large amount of detailed facial models. We show our pipeline in Figure 5 to predict a detailed and riggable 3D face model from a single image. The pipeline consists of three stages: base model fitting, displacement map prediction and dynamic details synthesis. We will explain each stage in detail in the following sections.

4.1. Base Model Fitting

The bilinear model for base shape is inherently riggable as the parametric space is separated into identity dimension and expression dimension, so the rough riggable model can be generated by regressing the parameters of identity for the bilinear model. Following [46], we estimate parameters corresponding to a given image by optimizing an objective function consisting of three parts. The first part is landmark alignment term. Assuming the camera is weak perspective, the landmark alignment term E_{lan} is defined as the distance between the detected 2D landmark and its corresponding vertex projected on the image space. The second part is pixel-level consistency term E_{pixel} measur-

ing how well the input image is explained by a synthesized image. The last part is regularization term which formulates identity, expression, and albedo parameters as multivariate Gaussians. The final objective function is given by:

$$E = E_{lan} + \lambda_1 E_{pixel} + \lambda_2 E_{id} + \lambda_3 E_{exp} + \lambda_4 E_{alb} \quad (2)$$

where E_{id} , E_{exp} and E_{alb} are the regularization terms of expression, identity and albedo, respectively. λ_1 , λ_2 , λ_3 and λ_4 are the weights of different terms.

After obtaining the identity parameter w_{id} , individual-specific blendshapes B_i can be generated as:

$$B_i = C_r \times w_{exp}^{(i)} \times w_{id}, 0 \leq i \leq 51 \quad (3)$$

where $w_{exp}^{(i)}$ is the expression parameter corresponding to blendshape B_i from Tucker decomposition.

4.2. Displacement Map Prediction

Detailed geometry is expressed by displacement maps for our predicted model. In contrast to the static detail which is only related to the specific expression in a certain moment, dynamic detail expresses the geometry details in varying expressions. Since the single displacement map cannot represent the dynamic details, we try to predict multiple displacement maps for 20 basic expressions in FaceScape using a deep neural network.

We observed that the displacement map in a certain expression could be decoupled into static part and dynamic part. The static part tends to keep static in different expressions, and is mostly related to the intrinsic feature like pores, nevus, and organs. The dynamic part varies in different expressions, and is related to the surface shrinking and stretching. We use a deforming map to model the surface motion, which is defined as the difference of vertices' 3D position from source expression to target expression in the UV space. As shown in Figure 4, we can see the variance between displacement maps is strongly related to the deforming map, and the static features in displacement maps are related to the texture. So we feed motion maps and textures to a CNN to predict the displacement map for multiple expressions.

We use pix2pixHD[53] as the backbone of our neural network to synthesize high resolution displacement maps. The input of the network is the stack of deforming map and texture in UV space, which can be computed from the recovered base model. Similar to [53], the combination of adversarial loss L_{adv} and feature matching loss L_{FM} is used to train our net with the loss function formulated as:

$$\min_G \left(\max_{D_1, D_2, D_3} \sum_{k=1,2,3} L_{adv}(G, D_k) \right) + \lambda \sum_{k=1,2,3} L_{FM}(G, D_k) \quad (4)$$

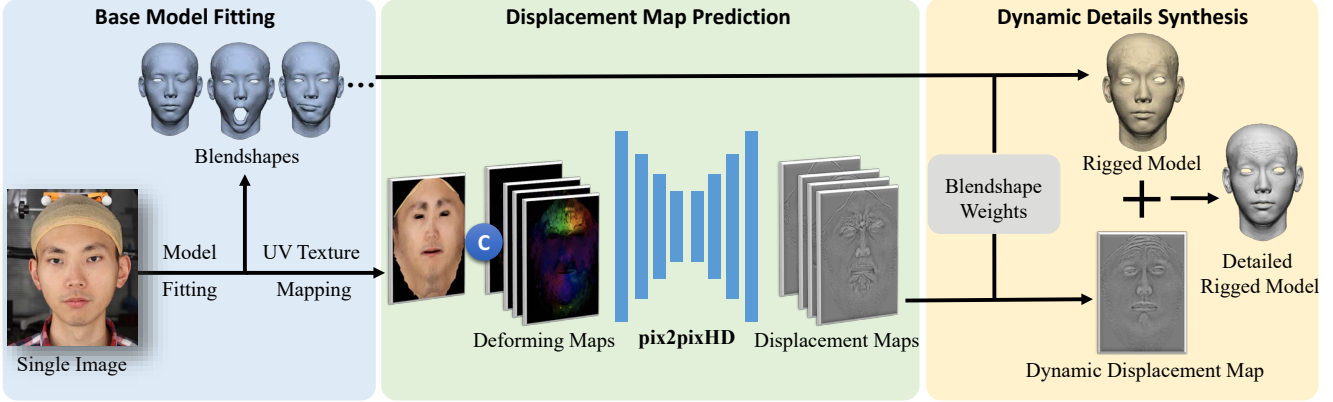


Figure 5: The pipeline to predict a detailed riggable 3D face from a single image consists of three stages: base model fitting, displacement map prediction, and dynamic details synthesis.

where G is the generator, D_1, D_2 and D_3 are discriminators that have the same LSGAN[32] architecture but operate at different scales, λ is the weight of feature matching loss.

4.3. Dynamic Detail Synthesis

Inspired by[33], we synthesize displacement map F for an arbitrary expression corresponding to specific blendshape weight α , using a weighted linear combination of generated displacement maps \hat{F}_0 in neutral expression and \hat{F}_i in other 19 key expressions:

$$F = M_0 \odot \hat{F}_0 + \sum_{i=1}^{19} M_i \odot \hat{F}_i \quad (5)$$

where M is the weight mask with the pixel value between 0 and 1, \odot is element-wise multiplication operation. To calculate the weight mask, considering the blendshape expressions change locally, we first compute an activation mask A_j in UV space for each blendshape mesh e_j as:

$$A_j(p) = \|e_j(p) - e_0(p)\|_2 \quad (6)$$

where $A_j(p)$ is the pixel value at position p of the j th activation mask, $e_j(p)$ and $e_0(p)$ is the corresponding vertices position on blendshape mesh e_j and neutral blendshape mesh e_0 , respectively. The activation masks are further normalized between 0 and 1. Given the activation mask A_j for each of the 51 blendshape meshes, the i th weight mask M_i is formulated as a linear combination of the activation masks weighted by the current blendshape weight α and fixed blendshape weight $\hat{\alpha}_i$ corresponding to the i th key expression:

$$M_i = \sum_{j=1}^{51} \alpha^j \hat{\alpha}_i^j A_j \quad (7)$$

where α^j is the j th element of α . M_0 is given by $M_0 = \max(0, 1 - \sum_{i=1}^{19} M_i)$.

There are many existing performance driven facial animation methods generating blendshape weights with depth camera[54, 29, 9] or single RGB camera[11, 10, 14]. As blendshape weights have semantic meaning, it's easy for artists to manually adjust the rigging parameters.

5. Experiments

5.1. Implement Detail

We use 888 people in our dataset as training data with a total of 17760 displacement maps, leaving 50 people for testing. We use the Adam optimizer to train the network with learning rate as $2e^{-4}$. The input textures and output displacement maps' resolution of our network is both 1024×1024 . We use 50 identity parameters, 52 expression parameters and 100 albedo parameters for our parametric model in all experiments.

5.2. Evaluation of 3D Model Prediction

The predicted riggable 3D faces are shown in Figure 6. To show riggable feature of the recovered facial model, we rig the model to 5 specific expressions. We can see the results of rigged models contain the photo-realistic detailed wrinkles, which cannot be recovered by previous methods. The point-to-plane reconstruction error is computed between our model and the ground-truth shape. The mean error is reported in Table 2. More results and the generated animations are shown in the supplementary material.

5.3. Ablation Study

W/O dynamic detail. We try to use only one displacement map from source image for rigged expressions, and the other parts remain the same. As shown in Figure 9, we find that the rigged model with dynamic detail shows the wrinkles caused by various expressions, which are not found in W/O dynamic method.

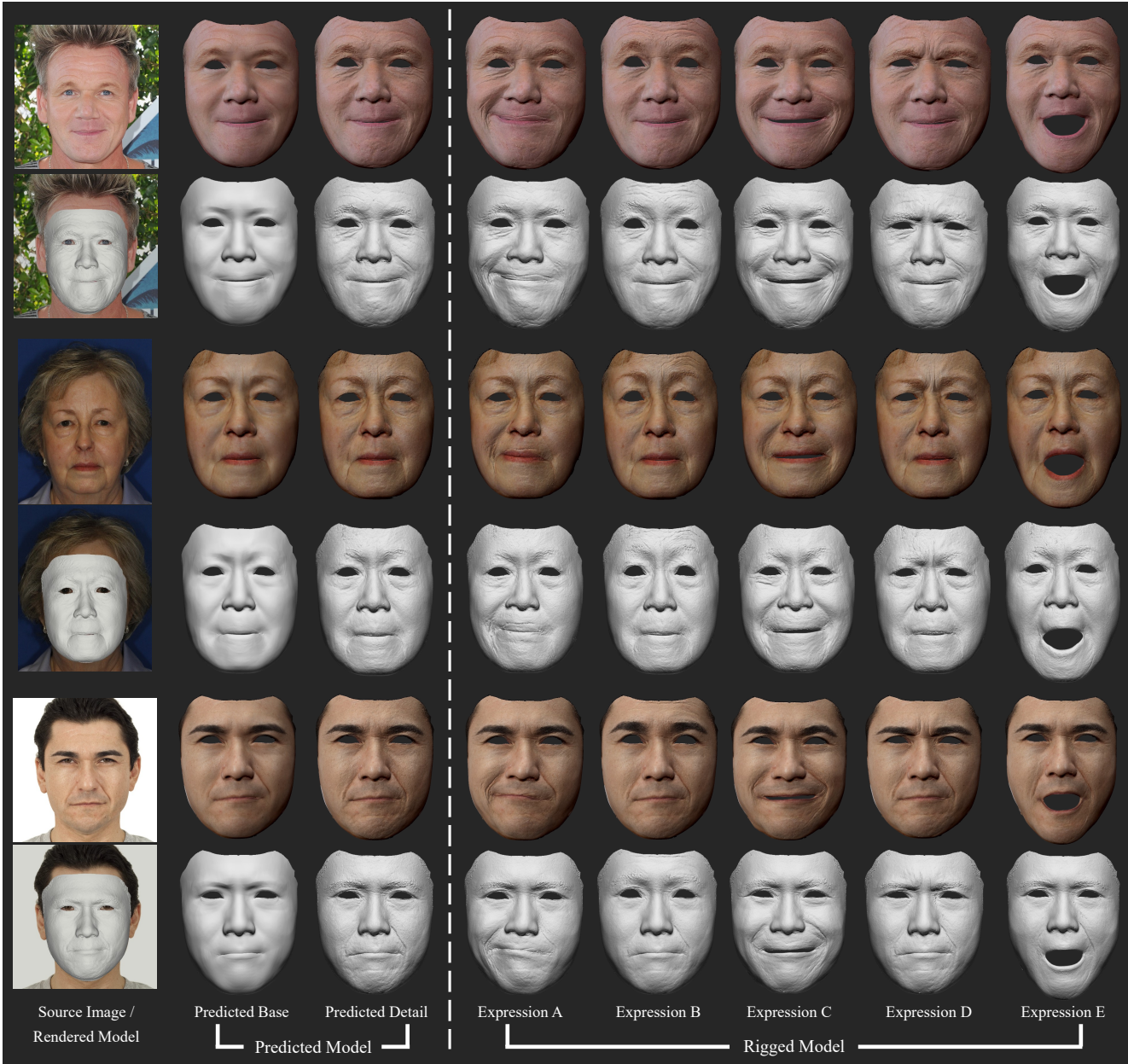


Figure 6: We show our predicted faces in source expression and rigged expressions. It is worth noting that the wrinkles in rigged expressions are predicted from the source image.

Table 2: 3D face Prediction Error

method	mean error	variance
our method (all exp.)	1.39	2.33
our method (source exp.)	1.22	1.17
DFDN[15] (source exp.)	2.19	3.20
Extreme3D[47] (source exp.)	2.06	2.55
3DDFA[62] (source exp.)	2.17	3.23

W/O deforming Map. We change the input of our displacement map prediction network by replacing the deforming map with one-hot encoding for each of 20 target expressions. As shown in Figure 9, we find the results without deforming map (W/O Def. Map) contain few details caused by expressions.

5.4. Comparisons to Prior Works

We show the predicted results of our result and other works in Figure 7. The comparison of detail prediction is

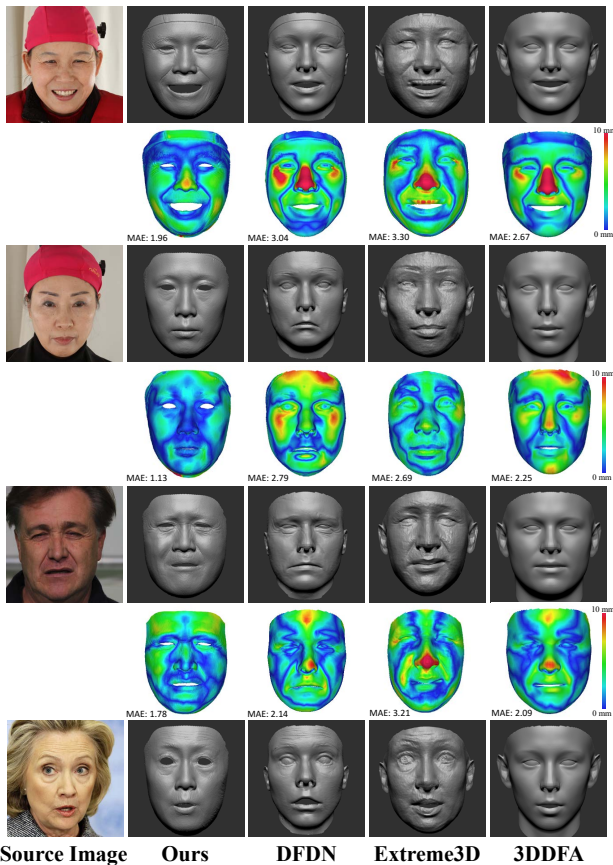


Figure 7: Comparison of static 3D face prediction with previous methods. The images in top two rows are from FaceScape, the image in third row is from volker sequence[51], and the image in bottom row is from Internet. The top three images are with ground truth shapes, so we evaluate the reconstruction error and show the heat map below each row. Our method predicts the lowest error comparing to three previous methods.

shown in Figure 8. As most of the detailed face predicted by other works cannot be directly rigged to other expressions, we only show the face shape in the source expression. Our results are visually better than previous methods, and also quantitatively better in the heat map of error. We consider the major reason for our method to perform the best in accuracy is the strong representation power of our bilinear model, and the predicted details contribute to the visually plausible detailed geometry.

6. Conclusion

We present a large-scale detailed 3D facial dataset, FaceScape. Comparing to previous public large-scale 3D face datasets, FaceScape provides the highest geometry quality and the largest model amount. We explore to pre-



Figure 8: Comparison of detail prediction. We adopt NICP[1] to register the base meshes of different methods to ground truth scans, and visualize the predicted details on common base meshes.

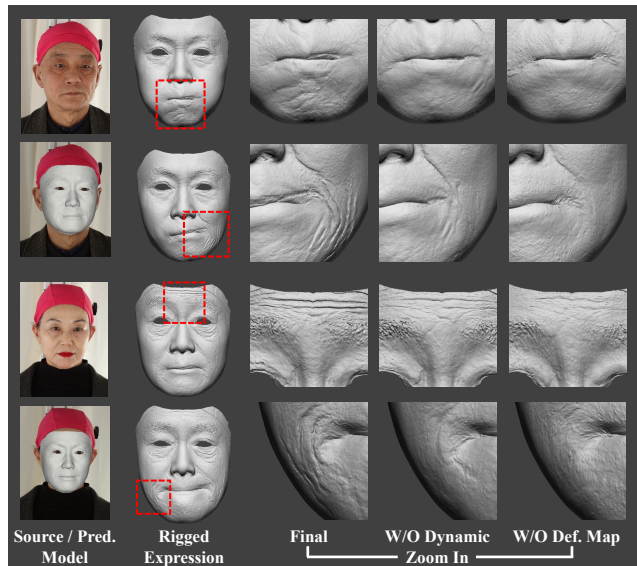


Figure 9: Ablation study. Our final model are able to recover wrinkles in rigged expressions, while the method W/O demforming map and W/O dynamic details cannot.

dict a detailed riggable 3D face model from a single image, and achieve high fidelity in dynamic detail synthesis. We believe the release of FaceScape will spur the future researches including 3D facial modeling and parsing.

Acknowledgements

This work was supported by the grants – NSFC 61627804 / U1936202, USDA 2018-67021-27416, JSNSF BK20192003, and a grant from Baidu Research.

References

- [1] Brian Amberg, Sami Romdhani, and Thomas Vetter. Optimal step nonrigid icp algorithms for surface registration. In *CVPR*, pages 1–8, 2007. 3, 8, 11
- [2] Timur Bagautdinov, Chenglei Wu, Jason Saragih, Pascal Fua, and Yaser Sheikh. Modeling facial geometry using compositional vaes. In *CVPR*, pages 3877–3886, 2018. 2
- [3] Yin Baocai, Sun Yanfeng, Wang Chengzhang, and Ge Yun. Bjut-3d large scale 3d face database and information processing. *Journal of Computer Research and Development*, 6:020, 2009. 2, 3
- [4] Volker Blanz, Thomas Vetter, et al. A morphable model for the synthesis of 3d faces. In *Siggraph*, volume 99, pages 187–194, 1999. 2
- [5] James Booth, Epameinondas Antonakos, Stylianos Ploumpis, George Trigeorgis, Yannis Panagakis, and Stefanos Zafeiriou. 3d face morphable models "in-the-wild". In *CVPR*, pages 5464–5473, 2017. 2
- [6] James Booth, Anastasios Roussos, Allan Ponniah, David Dunaway, and Stefanos Zafeiriou. Large scale 3d morphable models. *IJCV*, 126(2-4):233–254, 2018. 2
- [7] James Booth, Anastasios Roussos, Evangelos Ververas, Epameinondas Antonakos, Stylianos Ploumpis, Yannis Panagakis, and Stefanos Zafeiriou. 3d reconstruction of in-the-wild?faces in images and videos. *PAMI*, 40(11):2638–2652, 2018. 2
- [8] James Booth, Anastasios Roussos, Stefanos Zafeiriou, Allan Ponniah, and David Dunaway. A 3d morphable model learnt from 10,000 faces. In *CVPR*, pages 5543–5552, 2016. 1, 2
- [9] Sofien Bouaziz, Yangang Wang, and Mark Pauly. Online modeling for realtime facial animation. *ToG*, 32(4):40, 2013. 6
- [10] Chen Cao, Qiming Hou, and Kun Zhou. Displaced dynamic expression regression for real-time facial tracking and animation. *ToG*, 33(4):43, 2014. 6
- [11] Chen Cao, Yanlin Weng, Stephen Lin, and Kun Zhou. 3d shape regression for real-time facial animation. *ToG*, 32(4):41, 2013. 6
- [12] Chen Cao, Yanlin Weng, Shun Zhou, Yiyong Tong, and Kun Zhou. Facewarehouse: A 3d facial expression database for visual computing. *TVCG*, 20(3):413–425, 2013. 1, 2, 3, 4, 11, 12
- [13] Xun Cao, Zheng Li, and Qionghai Dai. Semi-automatic 2d-to-3d conversion using disparity propagation. *ToB*, 57(2):491–499, 2011. 2
- [14] Bindita Chaudhuri, Noranart Vesdapunt, and Baoyuan Wang. Joint face detection and facial motion retargeting for multiple faces. In *CVPR*, pages 9719–9728, 2019. 6
- [15] Zhang Chen, Guli Zhang, Ziheng Zhang, Kenny Mitchell, Jingyi Yu, et al. Photo-realistic facial details synthesis from single image. *arXiv preprint arXiv:1903.10873*, 2019. 3, 7
- [16] Shiyang Cheng, Michael Bronstein, Yuxiang Zhou, Irene Kotsia, Maja Pantic, and Stefanos Zafeiriou. Meshgan: Non-linear 3d morphable models of faces. *arXiv preprint arXiv:1903.10384*, 2019. 2
- [17] Shiyang Cheng, Irene Kotsia, Maja Pantic, and Stefanos Zafeiriou. 4dfab: A large scale 4d database for facial expression analysis and biometric applications. In *CVPR*, pages 5117–5126, 2018. 2, 3
- [18] Darren Cosker, Eva Krumerhuber, and Adrian Hilton. A face valid 3d dynamic action unit database with applications to 3d dynamic morphable facial modeling. In *ICCV*, pages 2296–2303, 2011. 2, 3
- [19] Hang Dai, Nick Pears, William AP Smith, and Christian Duncan. A 3d morphable model of craniofacial shape and texture variation. In *ICCV*, pages 3085–3093, 2017. 1
- [20] Pengfei Dou, Shishir K Shah, and Ioannis A Kakadiaris. End-to-end 3d face reconstruction with deep neural networks. In *CVPR*, pages 5908–5917, 2017. 2
- [21] Paul Ekman and Wallace V. Friesen. Facial action coding system: a technique for the measurement of facial movement. 1978. 4
- [22] John Flynn, Ivan Neulander, James Philbin, and Noah Snavely. Deepstereo: Learning to predict new views from the world's imagery. In *CVPR*, pages 5515–5524, 2016. 2
- [23] John C Gower. Generalized procrustes analysis. *Psychometrika*, 40(1):33–51, 1975. 11
- [24] Yudong Guo, Jianfei Cai, Boyi Jiang, Jianmin Zheng, et al. Cnn-based real-time dense face reconstruction with inverse-rendered photo-realistic face images. *PAMI*, 41(6):1294–1307, 2018. 2
- [25] Weicheng Huang, Xun Cao, Ke Lu, Qionghai Dai, and Alan Conrad Bovik. Toward naturalistic 2d-to-3d conversion. *TIP*, 24(2):724–733, 2014. 2
- [26] Loc Huynh, Weikai Chen, Shunsuke Saito, Jun Xing, Koki Nagano, Andrew Jones, Paul Debevec, and Hao Li. Mesoscopic facial geometry inference using deep neural networks. In *CVPR*, pages 8407–8416, 2018. 3
- [27] Zi-Hang Jiang, Qianyi Wu, Keyu Chen, and Juyong Zhang. Disentangled representation learning for 3d face shape. In *CVPR*, pages 11957–11966, 2019. 2
- [28] Hao Li, Thibaut Weise, and Mark Pauly. Example-based facial rigging. In *ToG*, volume 29, page 32, 2010. 2, 4
- [29] Hao Li, Jihun Yu, Yuting Ye, and Chris Bregler. Realtime facial animation with on-the-fly correctives. *ToG*, 32(4):42–1, 2013. 6
- [30] Tianye Li, Timo Bolkart, Michael J Black, Hao Li, and Javier Romero. Learning a model of facial shape and expression from 4d scans. *ToG*, 36(6):194, 2017. 2, 4
- [31] Marcel Lüthi, Thomas Gerig, Christoph Jud, and Thomas Vetter. Gaussian process morphable models. *PAMI*, 40(8):1860–1873, 2017. 2
- [32] Xudong Mao, Qing Li, Haoran Xie, Raymond YK Lau, Zhen Wang, and Stephen Paul Smolley. Least squares generative adversarial networks. In *ICCV*, pages 2794–2802, 2017. 6
- [33] Koki Nagano, Jaewoo Seo, Jun Xing, Lingyu Wei, Zimo Li, Shunsuke Saito, Aviral Agarwal, Jens Fursund, Hao Li, Richard Roberts, et al. pagan: real-time avatars using dynamic textures. *ToG*, 37(6):258–1, 2018. 6
- [34] Pascal Paysan, Reinhard Knothe, Brian Amberg, Sami Romdhani, and Thomas Vetter. A 3d face model for pose

- and illumination invariant face recognition. In *IEEE International Conference on Advanced Video and Signal Based Surveillance*, pages 296–301, 2009. 1, 2
- [35] P Jonathon Phillips, Patrick J Flynn, Todd Scruggs, Kevin W Bowyer, Jin Chang, Kevin Hoffman, Joe Marques, Jaesik Min, and William Worek. Overview of the face recognition grand challenge. In *CVPR*, pages 947–954, 2005. 1
- [36] Ravi Ramamoorthi and Pat Hanrahan. A signal-processing framework for inverse rendering. In *Proceedings of Conference on Computer Graphics and Interactive Techniques*, pages 117–128, 2001. 11
- [37] Elad Richardson, Matan Sela, Roy Orel, and Ron Kimmel. Learning detailed face reconstruction from a single image. In *CVPR*, pages 5553–5562, 2017. 2
- [38] Sami Romdhani and Thomas Vetter. Estimating 3d shape and texture using pixel intensity, edges, specular highlights, texture constraints and a prior. In *CVPR*, volume 2, pages 986–993, 2005. 2
- [39] Wojciech Sankowski, Piotr Stefan Nowak, and Paweł Krotewicz. Multimodal biometric database dmcsv1 of 3d face and hand scans. In *MIXDES*, pages 93–97, 2015. 2
- [40] Arman Savran, Neşe Alyüz, Hamdi Dibeklioğlu, Oya Çeliktutan, Berk Gökberk, Bülent Sankur, and Lale Akarun. Bosphorus database for 3d face analysis. In *European Workshop on Biometrics and Identity Management*, pages 47–56, 2008. 2, 3
- [41] Steven M Seitz, Brian Curless, James Diebel, Daniel Scharstein, and Richard Szeliski. A comparison and evaluation of multi-view stereo reconstruction algorithms. In *CVPR*, volume 1, pages 519–528, 2006. 2
- [42] Matan Sela, Elad Richardson, and Ron Kimmel. Unrestricted facial geometry reconstruction using image-to-image translation. In *ICCV*, pages 1576–1585, 2017. 2
- [43] Soumyadip Sengupta, Angjoo Kanazawa, Carlos D Castillo, and David W Jacobs. Sfsnet: Learning shape, reflectance and illuminance of faces in the wild. In *CVPR*, pages 6296–6305, 2018. 2
- [44] Robert W Sumner and Jovan Popović. Deformation transfer for triangle meshes. *ToG*, 23(3):399–405, 2004. 11
- [45] Ayush Tewari, Michael Zollhöfer, Pablo Garrido, Florian Bernard, Hyeonwoo Kim, Patrick Pérez, and Christian Theobalt. Self-supervised multi-level face model learning for monocular reconstruction at over 250 hz. In *CVPR*, pages 2549–2559, 2018. 2
- [46] Justus Thies, Michael Zollhofer, Marc Stamminger, Christian Theobalt, and Matthias Nießner. Face2face: Real-time face capture and reenactment of rgb videos. In *CVPR*, pages 2387–2395, 2016. 2, 5
- [47] Anh Tuan Tran, Tal Hassner, Iacopo Masi, Eran Paz, Yuval Nirkin, and Gérard G Medioni. Extreme 3d face reconstruction: Seeing through occlusions. In *CVPR*, pages 3935–3944, 2018. 2, 7
- [48] Luan Tran, Feng Liu, and Xiaoming Liu. Towards high-fidelity nonlinear 3d face morphable model. In *CVPR*, pages 1126–1135, 2019. 2
- [49] Luan Tran and Xiaoming Liu. Nonlinear 3d face morphable model. In *CVPR*, pages 7346–7355, 2018. 2
- [50] Luan Tran and Xiaoming Liu. On learning 3d face morphable model from in-the-wild images. *PAMI*, 2019. 2
- [51] Levi Valgaerts, Chenglei Wu, Andrés Bruhn, Hans-Peter Seidel, and Christian Theobalt. Lightweight binocular facial performance capture under uncontrolled lighting. *ToG*, 31(6):187–1, 2012. 8
- [52] Daniel Vlasic, Matthew Brand, Hanspeter Pfister, and Jovan Popović. Face transfer with multilinear models. In *ToG*, volume 24, pages 426–433, 2005. 2, 4, 12
- [53] Ting-Chun Wang, Ming-Yu Liu, Jun-Yan Zhu, Andrew Tao, Jan Kautz, and Bryan Catanzaro. High-resolution image synthesis and semantic manipulation with conditional gans. In *CVPR*, pages 8798–8807, 2018. 5
- [54] Thibaut Weise, Sofien Bouaziz, Hao Li, and Mark Pauly. Realtime performance-based facial animation. In *ToG*, volume 30, page 77, 2011. 6, 11
- [55] Lijun Yin, Xiaochen Chen, Yi Sun, Worm Tony, and J. Reale Michael. A high-resolution 3d dynamic facial expression database, 2008. In *FG*, volume 126, 2008. 2, 3
- [56] Lijun Yin, Xiaozhou Wei, Yi Sun, Jun Wang, and Matthew J Rosato. A 3d facial expression database for facial behavior research. In *FG*, pages 211–216, 2006. 2, 3
- [57] Xing Zhang, Lijun Yin, Jeffrey F Cohn, Shaun Canavan, Michael Reale, Andy Horowitz, Peng Liu, and Jeffrey M Girard. Bp4d-spontaneous: a high-resolution spontaneous 3d dynamic facial expression database. *Image and Vision Computing*, 32(10):692–706, 2014. 2, 3
- [58] Hao Zhu, Yebin Liu, Jingtao Fan, Qionghai Dai, and Xun Cao. Video-based outdoor human reconstruction. *TCSVT*, 27(4):760–770, 2016. 2
- [59] Hao Zhu, Yongming Nie, Tao Yue, and Xun Cao. The role of prior in image based 3d modeling: a survey. *Frontiers of Computer Science*, 11(2):175–191, 2017. 2
- [60] Hao Zhu, Hao Su, Peng Wang, Xun Cao, and Ruigang Yang. View extrapolation of human body from a single image. In *CVPR*, pages 4450–4459, 2018. 2
- [61] Hao Zhu, Xinxin Zuo, Sen Wang, Xun Cao, and Ruigang Yang. Detailed human shape estimation from a single image by hierarchical mesh deformation. In *CVPR*, pages 4491–4500, 2019. 2
- [62] Xiangyu Zhu, Zhen Lei, Stan Z Li, et al. Face alignment in full pose range: A 3d total solution. *PAMI*, 2017. 7
- [63] Xiangyu Zhu, Zhen Lei, Xiaoming Liu, Hailin Shi, and Stan Z Li. Face alignment across large poses: A 3d solution. In *CVPR*, pages 146–155, 2016. 2
- [64] Xiangyu Zhu, Zhen Lei, Junjie Yan, Dong Yi, and Stan Z Li. High-fidelity pose and expression normalization for face recognition in the wild. In *CVPR*, pages 787–796, 2015. 11

Supplementary

A. Animation

We recommend watching the supplementary video, where the FaceScape dataset is briefly introduced and the generated animations are shown. In the animation part, the 3D face model is predicted from a single wild image, then is rigged to the expressions captured by FaceShift[54]. As shown in the video, the face model predicted by our method can be rigged to various expressions while recovers the dynamic details, such as the wrinkles caused by expressions. We also use the same rigging parameters to drive 3 different predicted models, and find that they appear different dynamic details. This is because these details are related to the source subjects, not the rigging parameters.

B. Model Processing Details

The generation of topologically uniformed model has been briefly introduced in Section 3.2 of the main paper. Here we supplement a detailed description of model registration and displacement map generation.

Registration of base shape. We down-sample the raw recovered mesh into rough mesh with fewer triangle faces, namely base shape, and then build 3DMM for these simplified meshes. Firstly, the 2D landmarks are extracted from the frontal image, then the corresponding 3D landmarks are obtained by inverse-projection 2D landmarks. The Procrustes transformation[23] is used to register all landmarks to a standard 3D facial template with landmark annotations. In this way, the pose and scale for all the scanned meshes are roughly aligned to the standard facial template. Then we use Non-rigid ICP[1] to register the standard template mesh to scanned mesh in neutral expression. For scanned meshes in other 19 expressions, similar to [12], the deformation transfer algorithm[44] is firstly used to deform the registered mesh in neutral expression to other expressions mimicking the deformation of a set of template meshes in corresponding expressions. Then the Non-rigid ICP[1] is used to register these deformed individual-specific templates to scanned meshes to fit the scans in non-neutral expressions more accurately.

Displacement map generation. After obtaining the topology-uniformed base shape, we use displacement maps in UV space to represent middle and fine scale details that are not captured by the base model due to the small number of vertices and faces. The most straightforward way to compute the displacement map is to calculate the distance from the surface of the registered model to the raw mesh. However, we find that there will be artifacts in the displacement map caused by the defects in the registration procedure. Thus the raw scan is firstly smoothed with Laplacian mesh smoothing. Then we trace the surface points of

base mesh corresponding to pixels in the displacement map, and inverse-project the points to the raw mesh along normal direction to find its corresponding points. The pixel value of the displacement map is set to the signed distance from the point on raw mesh to its corresponding point on the smoothed mesh.

C. Base Model Fitting

The base model fitting method has been briefly introduced in Section 4.1 of the main paper. Here we provide a detailed description of three parts in the objective function.

Landmark Alignment. Firstly the 2D landmarks L are extracted from the image using an off-the-shelf facial landmark detector. Assuming the camera is weak perspective, the landmark alignment term is defined as the distance between the detected 2D landmark $L^{(k)}$ and its corresponding vertex projected on the image space:

$$E_{lan} = \|(sR(C_r \times \mathbf{w}_{exp} \times \mathbf{w}_{id})^{(k)} + \mathbf{t}) - L^{(k)}\|_2^2 \quad (8)$$

where s is the scale factor of the weak perspective function, R is the rotation matrix and \mathbf{t} is the translation.

Pixel Level Consistency. The pixel-level reconstruction term is used to match the geometry more accurately in the regions where no feature points such as cheeks exists. Under the assumption of Lambertian surfaces, we use the first three bands of Spherical Harmonics(SH)[36] for illumination representation. The per-vertex albedo is represented as a PCA model based on our dataset with albedo parameter \mathbf{w}_{alb} . The objective function is formulated as:

$$E_{pixel} = \frac{1}{|\mathcal{V}|} \sum_{q \in \mathcal{V}} \|\hat{I}(q) - I(q)\|_2 \quad (9)$$

where \mathcal{V} is the set of pixels corresponding to frontal vertices of the fitted mesh, \hat{I} is the synthetic face, I is the input image.

Regularization. We formulate the prior of identity, expression and albedo parameters as multivariate Gaussians around the average of our dataset for regularization. The final objective function is given by:

$$E = E_{lan} + \lambda_1 E_{pixel} + \lambda_2 E_{id} + \lambda_3 E_{exp} + \lambda_4 E_{alb} \quad (10)$$

where E_{id} , E_{exp} and E_{alb} are the regularization terms of expression, identity and albedo, respectively. λ_1 , λ_2 , λ_3 and λ_4 are the weights of different terms. We optimize the parameters alternatively. Following [64], the vertex indices corresponding to contour landmarks of the face are updated after each iteration.

D. Facial Capture System

The capturing system has been briefly introduced in Section 3.1 of the main paper. Here we supplement the pictures

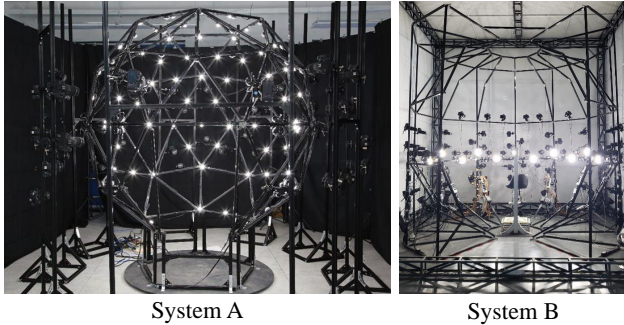


Figure 10: Our multi-view system to reconstruct the high quality detailed 3D face. We captured the data in two different places, so there are two frameworks shown as system A and system B.

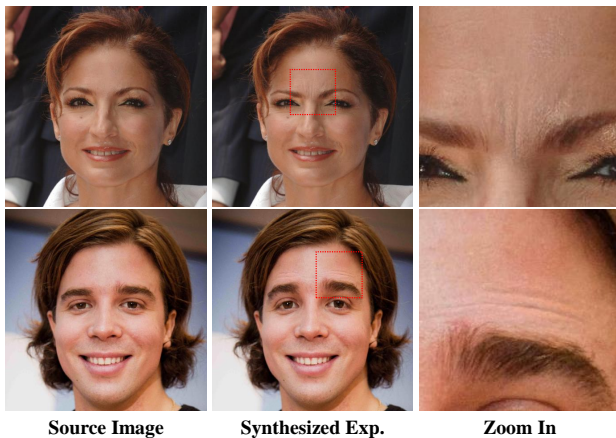


Figure 11: We use our recovered model for synthesizing images in another expression with detailed shading.



Figure 12: Failure cases. In the left, our prediction cannot recover the aquiline nose well, as this feature is not common in our dataset. In the right, the wrong displacement map is predicted due to occlusion.

of our system in Figure 10. The system consists of the 68 DSLR camera array, controlled lighting and a centralized control sever.

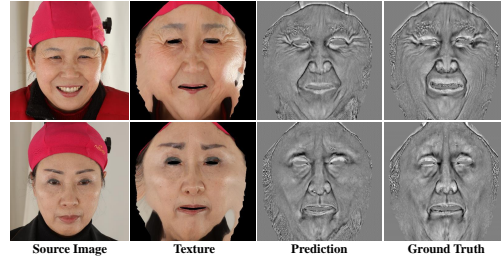


Figure 13: Predicted displacement maps using our method and ground truth.

E. More Results

More results are supplemented in Figure 14 as the extension of Figure 6 in our main paper. It shows that our results recover 3D faces with photo-realistic details. The faces can be further rigged to other expressions, and the details in the new expressions are synthesized to make the rigged model plausible.

We supplement the comparison of the predicted and ground-truth displacement maps in Figure 13 as the extension of Figure 7 in our main paper.

F. More Models

We show the 20 captured expressions for each subject in Figure 15, and show more subjects in neutral expression in Figure 16. The diversity of models in expression and identity dimensions ensures the quality of bilinear face model generated on FaceScape dataset.

G. Photo-realistic Image Synthesis

Similar to [52, 12], given a facial image, our bilinear model can be used to synthesize images in other expressions. Specifically, we use the base model fitting method to estimate the face model. Then we change the expression parameter to generate the face model in the target expression and warp the image pixels guided by translations of vertices on the 3D face model. The details caused by the expression changing are further synthesized by adjusting the pixel shading. New pixel value is calculated based on the new normal from the predicted displacement map and estimated illumination in model fitting procedure. The synthesized images are shown in Figure 11.

H. Failure Case

We show some failure cases of our method in Figure 12.

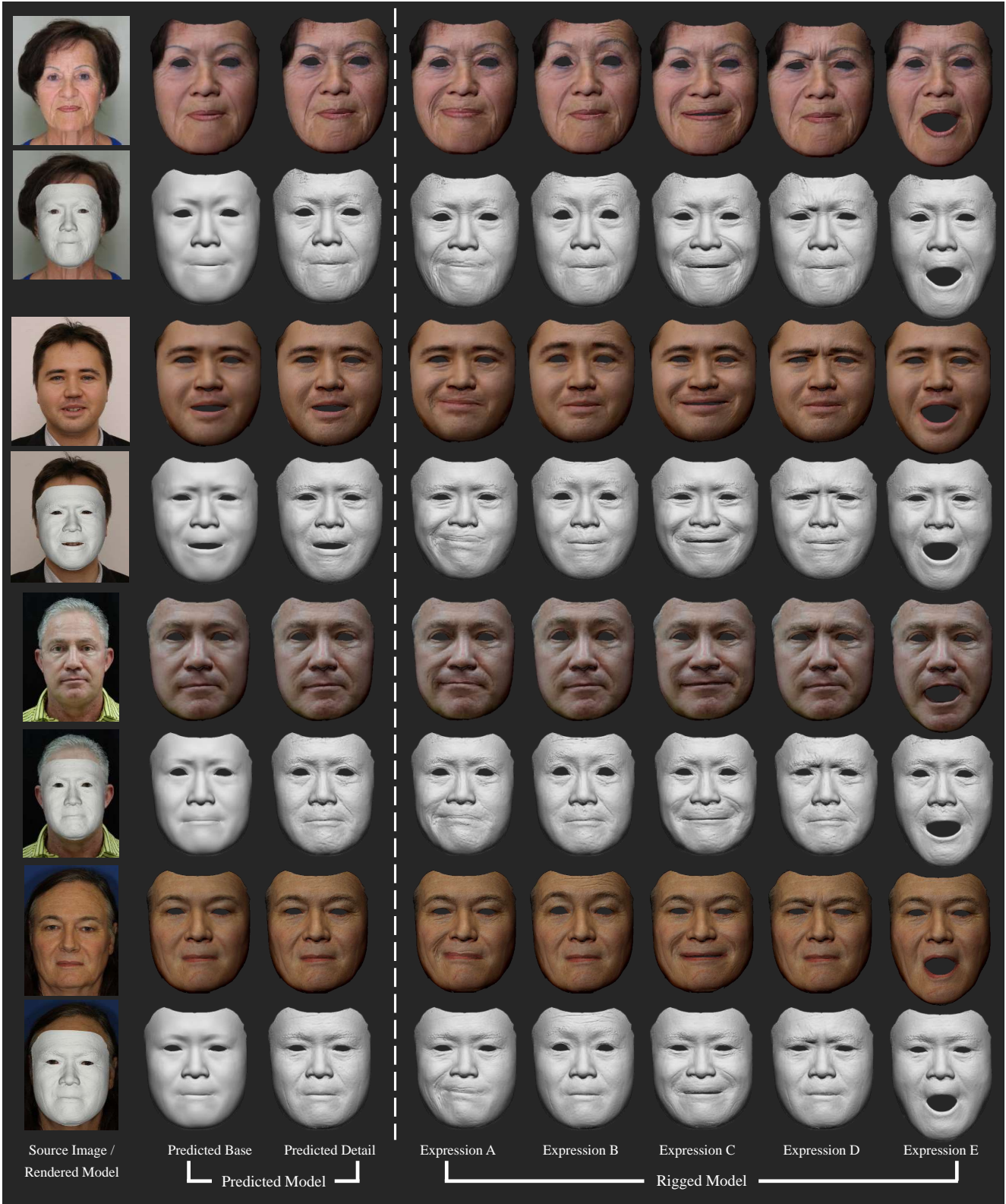


Figure 14: We show more results as the extension of Figure 6 in our main paper.

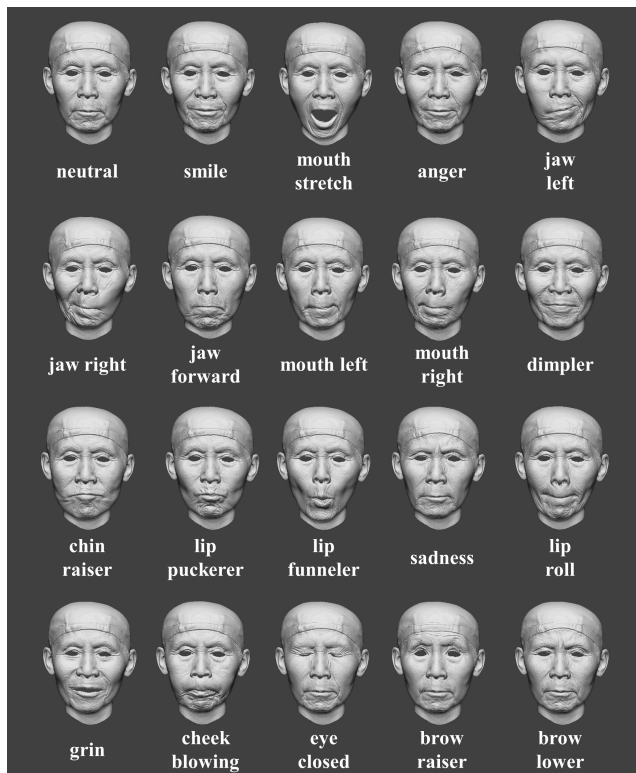


Figure 15: The 20 specified expressions which the subjects are asked to perform.

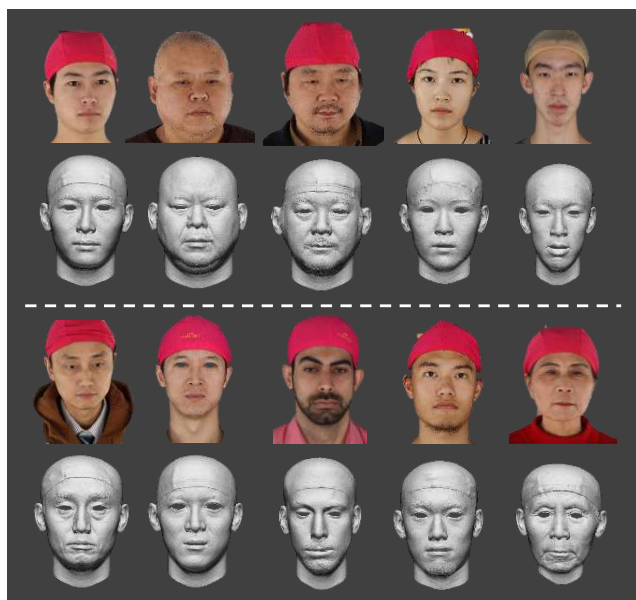


Figure 16: More models with different identities are shown in this figure. The upper part is the images of the subjects, and lower part is the processed topologically uniformed models.